

# Analysis of Crosstalk Problem in Multi-Twisted Bundle of Multi-Twisted Wire Based on BSAS-BP Neural Network Algorithm and Multilayer Transposition Method

Chao Huang<sup>1</sup>, Yang Zhao<sup>1\*</sup>, Wei Yan<sup>1,2</sup>, Qiangqiang Liu<sup>1</sup>, Jianming Zhou<sup>1</sup>,  
Zhaojuan Meng<sup>1</sup>, and Abdul Mueed<sup>1</sup>

<sup>1</sup> School of Electrical & Automation Engineering  
Nanjing Normal University, Nanjing 210046, China  
1547796467@qq.com, \*zhaoyang2@njnu.edu.cn, 61197@njnu.edu.cn, 1376684687@qq.com,  
386439740@qq.com, 1409352227@qq.com, engr.mueed@live.com

<sup>2</sup> Zhenjiang Institute for Innovation and Development  
Nanjing Normal University, Zhenjiang 212004, China

**Abstract** — Twisted wire used in complex systems has the ability to reduce electromagnetic interference, but crosstalk within the wire is not easy to obtain. This paper proposes a method to predict the crosstalk of multi-twisted bundle of multi-twisted wire (MTB-MTW). A neural network algorithm based on back propagation optimized by the beetle swarm antennae search method (BSAS-BPNN) is introduced to mathematically describe the relationship between the twist angle of the wire harness and the per-unit-length (p.u.l) parameter matrix. Considering the symmetry of the model, the relationship between the unresolved angle of the BSAS-BPNN algorithm and the p.u.l parameter matrix is processed by using the multilayer transposition method. Based on the idea of the cascade method and the finite-difference time-domain (FDTD) algorithm in Implicit-Wendroff format, the crosstalk of the wire is obtained. Numerical experiments and simulation results show that the new method proposed in this paper has better accuracy for the prediction of the model. The new method can be generalized to the MTB-MTW model with any number of wires. All theories provide preliminary theoretical basis for electromagnetic compatibility (EMC) design of high-band circuits.

**Index Terms** — Beetle swarm antennae search (BSAS) method, back propagation neural network (BPNN), crosstalk, multi-twisted bundle of multi-twisted wire (MTB-MTW), multilayer transposition method, multi-conductor transmission lines (MTLs).

## I. INTRODUCTION

Multi-conductor transmission lines used in aerospace and automotive machinery are particularly vulnerable to electromagnetic interference, but twisted wires have

been shown to improve anti-interference capabilities [1]. With the increase of the current operating frequency, the influence of crosstalk between wires cannot be ignored [2, 3].

This paper discusses an MTB-MTW model. The same wires are twisted into MTW, and multiple sets of MTWs are twisted into MTB-MTW. The MTB-MTW model will have regular twists along with the axis, and there will be corresponding changes in the p.u.l parameter matrix in the MTL equation [4]. Similar models have been proven to have high anti-interference ability, but the problem of crosstalk in its wire is not clear [5].

Recently, a large number of researchers have studied the prediction of twisted wire crosstalk [6]. Most researchers focus their research on the twisted wire pairs (TWP), while the research on twisted wires of multi-core harnesses is relatively few [7-9]. Other researchers have focused on the effects of externally applied excitation fields on MTB-TWP crosstalk [10, 11]. Traditional transmission line models are mostly parallel transmission lines, and crosstalk can be obtained by solving the transmission line equation directly [12]. The research method of non-uniform multi-conductor transmission line can be used as a reference to solve the crosstalk problem [13, 14]. According to the cascaded transmission line theory proposed by Paul and McKnight, cascaded multi-segment transmission lines are used to replace the overall harness [15-17]. The FDTD algorithm is also essentially a special cascaded transmission line method. The FDTD algorithm has been applied to the crosstalk problem of non-uniform transmission lines by some researchers [18, 19]. Therefore, as long as the p.u.l parameter matrix at different positions is obtained, the crosstalk of the wire harness can be obtained by the

FDTD method.

The different positions of MTB-MTW represent different twist angles, and the p.u.l parameter matrix is affected by the twist angle and the return plane. Considering the symmetry of MTB-MTW, the BPNN algorithm with strong non-linear mapping ability is introduced to mathematically describe the relationship between a part of the angle and the p.u.l parameter matrix [20, 21]. The dimension of the p.u.l parameter matrix will increase with the number of wire harnesses, so the result of the BPNN algorithm will fall into a local minimum. By introducing the BSAS method to optimize the BPNN, the global optimal value of the network is achieved [22, 23]. The relationship between the angles of the remaining parts and the p.u.l parameter matrix can be handled by the multilayer transposition method.

The structure of this paper is as follows. A model of MTB-MTW is established in Section II. In Section III, the extraction method of p.u.l parameter matrix and the prediction process of crosstalk are introduced. In Section IV, the new method is verified by numerical experiments using the MTB-MTW model, and the near-end and far-end crosstalk results are analyzed. The conclusions are given in Section V.

## II. MTB-MTW GEOMETRIC MODEL AND ITS MTL MODEL

### A. Geometric model of the MTB-MTW

The MTB-MTW cable bundle is a uniform twisted wire bundle, and its inner  $N$  group cable bundle contains an  $n$ -core uniform twisted wire. The twist direction of the  $n$ -core twisted wire and the  $N$  group of cable bundles is opposite. The materials of the  $N$  sets of cable bundles are all the same, with a total of  $nN$  core wires.

The MTB-MTW model is shown in Fig. 1. From the outer cable bundle (MTB-MTW), the transmission line can be divided into  $S^1$  identical small segments, and from the inner  $n$ -core stranded wire bundle (MTW) can be further divided into  $S^2$  identical small segments according to its twisted condition:

$$S = \frac{S^2}{S^1}, \quad (1)$$

where  $S$  represents the twisting ratio of MTB-MTW. It means that in each  $S_i^1$ , the  $n$ -core twisted wire in the inner layer will twist  $S$  segments.

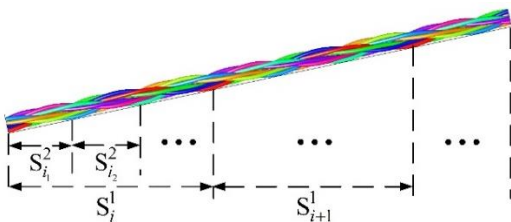


Fig. 1. Segmentation of MTB-MTW.

Since the models of  $S^1$  segments are all the same, only 1 segment needs to be considered. Using the idea of the cascade method, a model of the entire transmission line can be obtained.

For the convenience of description, three groups of cable bundles composed of three core wires are used as examples. The MTB-MTW model and the corresponding cross-section model are shown in Fig. 2. The model takes  $S=3$ . After the outer cable bundle (MTB-MTW) is twisted for one turn, the corresponding inner core 3-core twisted wire (MTW) is twisted for 3 turns.

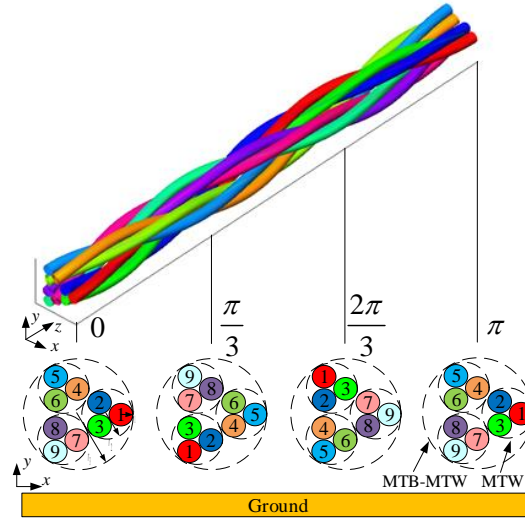


Fig. 2. Cable bundle and section model of MTB-MTW.

The position coordinates of each core are as follows:

$$\begin{cases} x_i = (r_3 - r_2) \cos\left\{\frac{360}{N} N(i) + \theta_1\right\} \\ \quad + (r_2 - r_1) \cos\left\{\frac{360}{n} n(i) + \theta_2\right\} \\ y_i = (r_3 - r_2) \sin\left\{\frac{360}{N} N(i) + \theta_1\right\}, \\ \quad + (r_2 - r_1) \sin\left\{\frac{360}{n} n(i) + \theta_2\right\} \\ z_i = \rho \theta_1 \end{cases}, \quad (2)$$

among them,  $r_1$  represents the radius of the core wire,  $r_2$  represents the radius of MTW,  $r_3$  represents the radius of MTB-MTW, and  $\rho$  represents the twist level of the cable bundle.  $N(i)$  and  $n(i)$  are the twisting degrees of MTB-MTW and MTW, respectively.  $\theta_1$  and  $\theta_2$  represent the twist angles of the outer and inner wire harnesses relative to the reference ground, respectively. According to formula (1) and the opposite twist direction of the inner and outer layers, it can be seen that it satisfies formula (3):

$$\theta_2 = (S-1)\theta_1. \quad (3)$$

Based on the above analysis, the model of Fig. 2 and the coordinates of formula (2) are generalized to the overall transmission line. MTB-MTW model was established out.

### B. MTL model of the MTB-MTW

The established MTB-MTW model is divided uniformly. Each small segment is regarded as a parallel transmission line according to the idea of the cascade method. The multi-conductor transmission line model of its unit length is shown in Fig. 3.  $r_{ij}$ ,  $l_{ij}$ ,  $c_{ij}$ , and  $g_{ij}$  represent the elements in the parameter matrix of resistance  $\mathbf{R}$ , inductance  $\mathbf{L}$ , capacitance  $\mathbf{C}$ , and conductance  $\mathbf{G}$ , respectively, where  $i, j = 1, 2, \dots, nN$ .

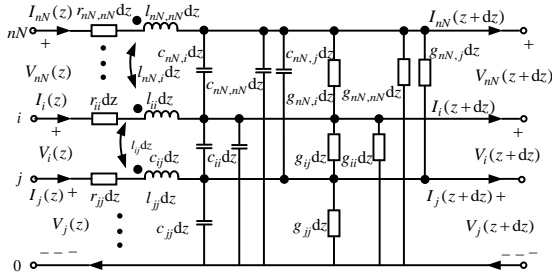


Fig. 3. MTL model of MTB-MTW.

Its satisfied transmission line equation [12]:

$$\begin{aligned} \frac{\partial \mathbf{V}(z,t)}{\partial z} + \mathbf{R}(z)\mathbf{I}(z,t) + \mathbf{L}(z) \frac{\partial \mathbf{I}(z,t)}{\partial t} &= 0 \\ \frac{\partial \mathbf{I}(z,t)}{\partial z} + \mathbf{G}(z)\mathbf{V}(z,t) + \mathbf{C}(z) \frac{\partial \mathbf{V}(z,t)}{\partial t} &= 0, \end{aligned} \quad (4)$$

where  $\mathbf{V}(z,t)$  and  $\mathbf{I}(z,t)$  are the voltage and current vectors at different positions and different times on the transmission lines, both of which are  $n$ -dimensional. The  $\mathbf{R}(z)$ ,  $\mathbf{L}(z)$ ,  $\mathbf{C}(z)$  and  $\mathbf{G}(z)$  parameter matrices are variables related to the position  $z$  of the transmission lines, and they are all  $n \times n$  order matrices.

For simplicity, the four p.u.l parameter matrices can be expressed as:

$$\mathbf{M} = \begin{bmatrix} m_{11} & m_{12} & \cdots & m_{1,nN} \\ m_{21} & m_{22} & \cdots & m_{2,nN} \\ \vdots & \vdots & \ddots & \vdots \\ m_{nN,1} & m_{nN,2} & \cdots & m_{nN,nN} \end{bmatrix}, \quad (5)$$

where  $\mathbf{M}$  represents different  $\mathbf{R}$ ,  $\mathbf{L}$ ,  $\mathbf{C}$  and  $\mathbf{G}$  parameter matrices.  $m_{ij}$  represents the corresponding parameter matrix specific resistance  $r_{ij}$ , inductance  $l_{ij}$ , capacitance  $c_{ij}$  and conductance  $g_{ij}$ . The p.u.l parameter matrices at different positions represent different matrices  $\mathbf{M}$ .

## III. PREDICTION OF PER-UNIT-LENGTH PARAMETER AND CROSSTALK

### A. Predicting p.u.l parameter by BSAS-BPNN algorithm

For MTB-MTW harnesses, different positions

represent different twist angles  $\theta_1$ , and the corresponding p.u.l parameter matrices are also different. Combining (2) and (3), there is a functional relationship between the parameter matrix  $\mathbf{M}$  and the twist angle  $\theta_1, \theta_2$ :

$$\mathbf{M}(\theta_1, \theta_2) = f(\theta_1). \quad (6)$$

Therefore, this paper introduces a BSAS-BP neural network algorithm with strong non-linear mapping capabilities, in which the BSAS algorithm is used to optimize the weight of the BPNN [23]. Its network topology is shown in Fig. 4.

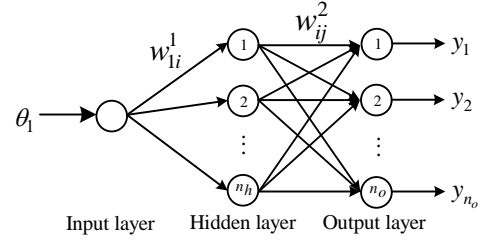


Fig. 4. Network topology of BSAS-BPNN.

The input of the network is the twist angle  $\theta_1$  at different positions. Considering the axis symmetry of the MTB-MTW model,  $\theta_1 \in [0^\circ, 360^\circ/N)$ . The parameter matrices in the other angular ranges can be obtained through part B. The output is a symmetric parameter matrix at this position, which can be represented by the vector  $Y$  as:

$$Y = [\bar{M}] = [y_1, y_2, \dots, y_{n_o}], \quad (7)$$

where  $\bar{M}$  is a row vector arranged by triangular elements on the parameter matrix.

The number of output layers  $n_o$  is determined by the parameter matrix RLCG, and the number of hidden layers  $n_h$  is an empirical value determined by the number of input layers and output layers, which is usually as follows:

$$n_h = 0.5(n_o + 1) + a, \quad a = 1, 2, \dots, 10. \quad (8)$$

BSAS algorithm is used to optimize the weights  $w_{li}^1$  and  $w_{ij}^2$ . Specific steps are as follows.

*Step 1:* Determine the optimized objective function. The output of the network is:

$$y_j = \sum_{i=1}^{n_h} \frac{w_{ij}^2}{1 + e^{-w_{li}^1 \theta_1}}. \quad (9)$$

For  $N$  sets of data, the mean square error between the network output value and the actual value is:

$$f(w) = E(w_{li}^1, w_{ij}^2) = \frac{1}{2N} \sum_{i=1}^N \sum_{j=1}^{n_o} (y_j - y'_j)^2, \quad (10)$$

where  $y'_j$  is the data value of the parameter matrix actually given, and all the weights are listed as a single row vector  $w$ .  $f(w)$  is the objective function to be

optimized.

*Step 2:* Initialize the beetle position vector  $w$  and the optimal value  $f_{best}$  of the objective function:

$$w^{(0)} = \text{rands}(k, 1), \quad (11)$$

where  $w$  represents the initial position of the beetle in the high-dimensional data space.  $k$  represents the dimension of the weight vector, and  $\text{rands}$  represents the generation of a uniformly distributed row vector.

*Step 3:* The direction ( $dir$ ) and position ( $w$ ) of  $M$  group beetles are randomly generated:

$$\begin{cases} dir_n^{(t)} = \frac{\text{rands}(k, 1)}{\|\text{rands}(k, 1)\|_2}, \\ w_n^{(t)} = w_n^{(t-1)} + dir_n^{(t)}, \end{cases} \quad (12)$$

where  $t = 0, 1, 2, \dots, n = 1, 2, \dots, M$ .

*Step 4:* Obtaining the optimal objective function value and updating the beetle's position.

When  $\min(f(w_n^{(t)})) \leq f_{best}^{(t)}$ ,

$$\begin{cases} f_{best}^{(t+1)} = \min_{1 \leq n \leq M} (f(w_n^{(t)})) \\ w^{(t+1)} = \arg \min_{1 \leq n \leq M} (f(w_n^{(t)})) \end{cases} \quad (13)$$

When  $\min(f(w_n^{(t)})) > f_{best}^{(t)}$ , the left and right beard positions of beetle can be calculated by the following formula (14):

$$\begin{cases} w_n^{(t)}(r) = w_n^{(t)} + \frac{d}{2} \cdot dir_n^{(t)} \\ w_n^{(t)}(l) = w_n^{(t)} - \frac{d}{2} \cdot dir_n^{(t)} \end{cases}, \quad (14)$$

where  $d$  is the distance between the left and right beards.

*Step 5:* The objective function value of the left and right beards can be calculated by the following formula:

$$\begin{cases} f_n^r = f_n(w_n^{(t)}(r)) \\ f_n^l = f_n(w_n^{(t)}(l)) \end{cases}, \quad (15)$$

$$w_n^{(t+1)} = w_n^{(t)} - \delta \cdot dir_n^{(t)} \cdot \text{sign}(f_n^r - f_n^l), \quad (16)$$

where  $\delta$  is the step size of the beetle, which is generally taken as  $\sqrt{k}$ , and  $\text{sign}$  represents the sign function.

*Step 6:* In summary, the objective function and the position of the beetle can be obtained:

$$\begin{cases} f_{best}^{(t+1)} = f_{best}^{(t)} \\ w^{(t+1)} = \arg \min_{1 \leq n \leq M} (f(w_n^{(t+1)})) \end{cases} \quad (17)$$

For the new  $w^{(t+1)}$ , the position of the beetle in each search direction can be obtained, and the next iteration calculation is performed.

Until iteration to the maximum number of iterations, the global minimum of the average error can be obtained. The process of BSAS optimizing the weight of BPNN is shown in Fig. 5.

The trained BSAS-BPNN algorithm can predict the parameter matrix at the corresponding position of

$0 \sim 360^\circ/N$ . However, the BSAS-BPNN algorithm cannot predict the parameter matrix at each position on the transmission line.

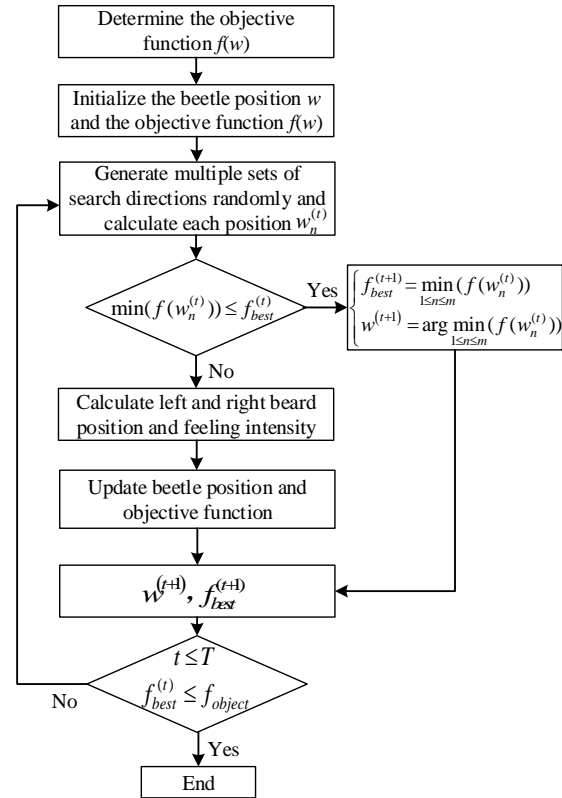


Fig. 5. BSAS algorithm to optimize the weight of BPNN.

## B. Multilayer transposition method to obtain p.u.l parameter at arbitrary positions

The parameter matrix at the corresponding position of  $0 \sim 360^\circ/N$  has been predicted by the BSAS-BPNN algorithm. Considering the symmetry of the MTB-MTW cable and the periodicity of the twist angle, the parameter matrix at the corresponding position of  $360^\circ/N \sim 360^\circ$  can be obtained by the multilayer transposition method.

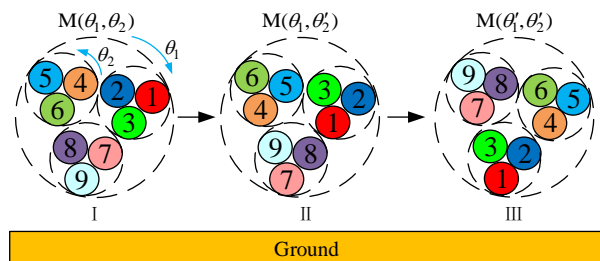


Fig. 6. Parameter matrix transformation between different positions and the same cross-section model.

The transformation process of the parameter matrix

at different positions and the same section is shown in Fig. 6. This means that the cross-section corresponding to any angle in  $360^\circ/N \sim 360^\circ$  ( $\theta'_1 \in [360^\circ/N, 360^\circ)$ ), the same cross-section model can always be found in  $0 \sim 360^\circ/N$  ( $\theta_1 \in [0^\circ, 360^\circ/N)$ ). Although the parameter matrices between the two cross-section models are not the same, but the transformation shown in Fig. 6 is also satisfied.

The parameter matrix  $\mathbf{M}$  is represented as a block matrix with respect to the MTB-MTW:

$$\mathbf{M} = \begin{bmatrix} \mathbf{M}_{n \times n}^{11} & \mathbf{M}_{n \times n}^{12} & \cdots & \mathbf{M}_{n \times n}^{1N} \\ \mathbf{M}_{n \times n}^{21} & \mathbf{M}_{n \times n}^{22} & \cdots & \mathbf{M}_{n \times n}^{2N} \\ \vdots & \vdots & \ddots & \vdots \\ \mathbf{M}_{n \times n}^{N1} & \mathbf{M}_{n \times n}^{N2} & \cdots & \mathbf{M}_{n \times n}^{NN} \end{bmatrix}, \quad (18)$$

$$\mathbf{M}_{n \times n}^{ij} = \begin{bmatrix} m_{n(i-1)+1, n(j-1)+1} & m_{n(i-1)+1, n(j-1)+2} & \cdots & m_{n(i-1)+1, nj} \\ m_{n(i-1)+2, n(j-1)+1} & m_{n(i-1)+2, n(j-1)+2} & \cdots & m_{n(i-1)+2, nj} \\ \vdots & \vdots & \ddots & \vdots \\ m_{ni, n(j-1)+1} & m_{ni, n(j-1)+2} & \cdots & m_{ni, nj} \end{bmatrix}, \quad (19)$$

where  $\mathbf{M}_{n \times n}^{ij}$  represents the parameter matrix between the MTB of the  $i$ -th and  $j$ -th bundle.  $n$  and  $N$  are the numbers of MTW and MTB, respectively. Because  $\mathbf{M}$  is a symmetric matrix, we know  $\mathbf{M}_{n \times n}^{ij} = (\mathbf{M}_{n \times n}^{ji})^T$ .

The initial cross-section I is transformed to a cross-section II in Fig. 6. At this time, no twists occurred in MTB. Considering only the twist angle of the MTW, the corresponding transformation is:

$$\mathbf{M}_{n \times n}^{ii}(\theta_1, \theta'_2) = \mathbf{T}_n^\alpha \mathbf{M}_{n \times n}^{ii}(\theta_1, \theta_2) \mathbf{T}_n^\alpha, \quad (20)$$

where  $\mathbf{M}_{n \times n}^{ii}(\theta_1, \theta_2)$  represents the parameter matrix of the cross-section I between the wire in the  $i$ -th bundle, and  $\mathbf{M}_{n \times n}^{ii}(\theta_1, \theta'_2)$  represents the parameter matrix of the corresponding cross-section II.  $\mathbf{T}_n$  represents the transformation matrix of  $n$ -core MTW under  $360^\circ/n$  twisting.  $\alpha$  is the number of twists of MTW:

$$\theta'_2 = \alpha \frac{360^\circ}{n} + \theta_2. \quad (21)$$

The mutual parameter matrix  $\mathbf{M}_{n \times n}^{ij}(\theta_1, \theta'_2)$  between the wires in the  $i$ -th and  $j$ -th bundles also satisfies the above transformation:

$$\mathbf{M}_{n \times n}^{ij}(\theta_1, \theta'_2) = \mathbf{T}_n^\alpha \mathbf{M}_{n \times n}^{ij}(\theta_1, \theta_2) \mathbf{T}_n^\alpha. \quad (22)$$

According to equations (20) and (22), the parameter matrix of cross-section II can be obtained as:

$$\mathbf{M}(\theta_1, \theta'_2) = [\mathbf{M}_{n \times n}^{ij}(\theta_1, \theta'_2)]_{N \times N}. \quad (23)$$

But cross-section II is just a virtual cross-section for the convenience of description. The final cross-section III can be transformed on the basis of cross-section II. The transformation of its parameter matrix is as follows:

$$\mathbf{M}(\theta'_1, \theta'_2) = \mathbf{P}_N^\beta \mathbf{M}(\theta_1, \theta'_2) \mathbf{P}_N^\beta, \quad (24)$$

where  $\mathbf{M}(\theta'_1, \theta'_2)$  is the parameter matrix of cross-

section III, and  $\mathbf{P}_N$  is the transformation matrix of MTB-MTW under  $360^\circ/N$  twisting. The MTB-MTW twisting times  $\beta$  satisfy:

$$\theta'_1 = \beta \frac{360^\circ}{N} + \theta_1. \quad (25)$$

Combining formulas (3), (21), and (25) shows:

$$\alpha = \frac{n(S-1)}{N} \beta. \quad (26)$$

Different  $n$  and  $N$  correspond to different transformation matrices  $\mathbf{T}_n$  and  $\mathbf{P}_N$ . In the MTB-MTW model of  $n=N=3$  discussed in this paper,  $\mathbf{T}_n$  and  $\mathbf{P}_N$  are:

$$\mathbf{T}_3 = \begin{bmatrix} 0 & 0 & 1 \\ 1 & 0 & 0 \\ 0 & 1 & 0 \end{bmatrix}, \mathbf{P}_3 = \begin{bmatrix} 0_{3 \times 3} & 0_{3 \times 3} & 1_{3 \times 3} \\ 1_{3 \times 3} & 0_{3 \times 3} & 0_{3 \times 3} \\ 0_{3 \times 3} & 1_{3 \times 3} & 0_{3 \times 3} \end{bmatrix}. \quad (27)$$

### C. Solving MTL equations and crosstalk

Combining parts A and B, the p.u.l parameter matrix at any position on the MTL model of MTB-MTW can be obtained. Discrete the MTL equation (4) as [24]:

$$\begin{cases} \mathbf{V}_k^t - \mathbf{V}_{k+1}^t + \mathbf{A}_{vk}(\mathbf{I}_k^t + \mathbf{I}_{k+1}^t) = \mathbf{V}_{k+1}^{t-1} - \mathbf{V}_k^{t-1} + \mathbf{B}_{vk}(\mathbf{I}_k^{t-1} + \mathbf{I}_{k+1}^{t-1}) \\ \mathbf{I}_k^t - \mathbf{I}_{k+1}^t + \mathbf{A}_{ik}(\mathbf{V}_k^t + \mathbf{V}_{k+1}^t) = \mathbf{I}_{k+1}^{t-1} - \mathbf{I}_k^{t-1} + \mathbf{B}_{ik}(\mathbf{V}_k^{t-1} + \mathbf{V}_{k+1}^{t-1}) \end{cases}. \quad (28)$$

The correlation matrix is:

$$\begin{aligned} \mathbf{V}_k^t &= \mathbf{V}(k\Delta z, t\Delta t), \quad \mathbf{I}_k^t = \mathbf{I}(k\Delta z, t\Delta t) \\ \mathbf{A}_{vk} &= -\left(\frac{\mathbf{R}(z_k)}{2} + \frac{\mathbf{L}(z_k)}{\Delta t}\right)\Delta z, \mathbf{B}_{vk} = \left(\frac{\mathbf{R}(z_k)}{2} - \frac{\mathbf{L}(z_k)}{\Delta t}\right)\Delta z \\ \mathbf{A}_{ik} &= -\left(\frac{\mathbf{G}(z_k)}{2} + \frac{\mathbf{C}(z_k)}{\Delta t}\right)\Delta z, \mathbf{B}_{ik} = \left(\frac{\mathbf{G}(z_k)}{2} - \frac{\mathbf{C}(z_k)}{\Delta t}\right)\Delta z, \end{aligned} \quad (29)$$

where  $\Delta z$  and  $\Delta t$  represent the length of space division and time division respectively.

According to the p.u.l parameter matrix at different positions,  $\mathbf{V}(z, t)$  and  $\mathbf{I}(z, t)$  at different positions and times can be iteratively obtained through equations (28) and (29).

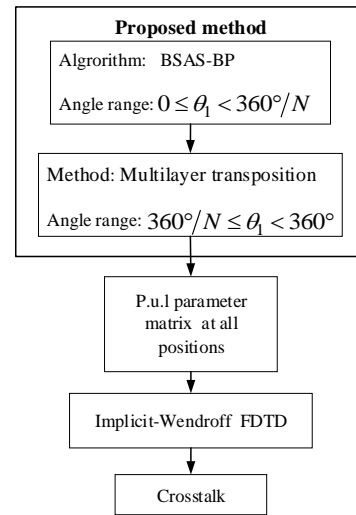


Fig. 7. Crosstalk prediction process of MTB-MTW.

## IV. VERIFICATION AND ANALYSIS

### A. Verification of BSAS-BPNN algorithm

In order to verify the correctness of the method proposed in this paper, an MTB-MTW cable with  $n=N=3$  is taken as an example to verify the new method. The wires in the model are copper wires with a diameter of 0.8mm. The wire insulation material is polyvinyl chloride (PVC), which has a thickness of 0.6 mm and a relative dielectric constant of 2.7. The length of the wire is 1m along the axial direction, and 50 ohm resistors are connected to both ends of the wire. Some related parameters are shown in Table 1.

Table 1: Related parameters

Name	Value
Wire diameter	0.8mm
Conductivity of the wire	58000000 S/m
Insulation layer thickness	0.6mm
Wire length	1m
Height of center wire from ground	15mm
Twist ratio	3
Number of MTB ( $N$ )	3
Number of MTW ( $n$ )	3

The initial reference cross-section model is as shown in Fig. 6 (cross-section I), and the p.u.l parameter matrix is extracted using ANSYS simulation software [25]. Figure 8 shows the error  $E$  iteration process of the BSAS-BPNN algorithm for four p.u.l parameter matrices. The units of the four p.u.l parameter matrices are  $\Omega/m$ , nH/m, pF/m, and mS/m. The corresponding iteration errors reach  $4 \times 10^{-6}$ ,  $5 \times 10^{-3}$ ,  $1 \times 10^{-3}$ , and  $2.5 \times 10^{-7}$ , respectively. Figure 9 shows the average error value of the p.u.l parameter matrix at 10 randomly selected angles, the maximum of which is less than 0.2%.

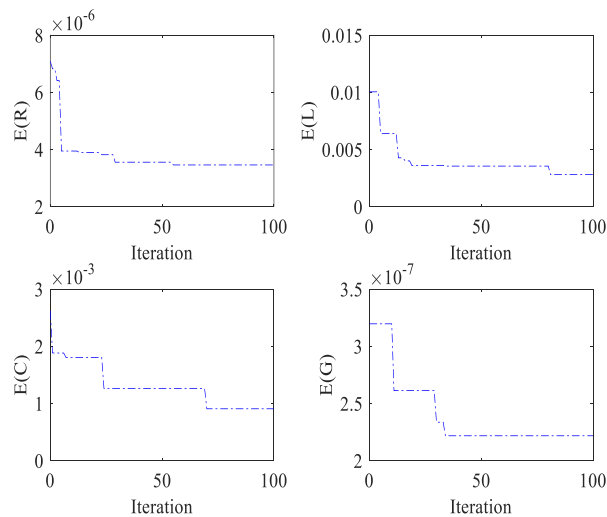


Fig. 8. Error iteration process of BSAS-BPNN algorithm.

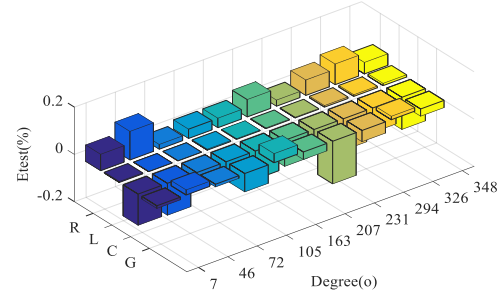


Fig. 9. Mean error of p.u.l parameter matrix.

### B. Analysis of crosstalk results

Simulation was performed using CST Cable Studio software based on the transmission line matrix (TLM) method. It is a high-precision numerical calculation method of electromagnetic field, which has high reference value [26]. Its arrangement in CST is shown in Fig. 10.

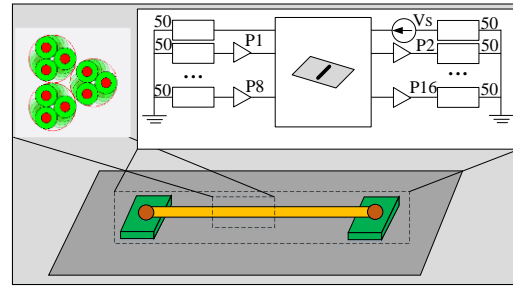


Fig. 10. Full-wave simulation experiment schematic diagram.

Near-end crosstalk (NEXT) and far-end crosstalk (FEXT) of each line are defined as follows:

$$NEXT_i = 20 \log_{10} \frac{V_{i,NEXT}}{V_S}, FEXT_i = 20 \log_{10} \frac{V_{i,FEXT}}{V_S}, \quad (30)$$

where  $V_S$  represents the applied interference voltage on line 1,  $V_{i,NEXT}$  represents the disturbed voltage of the  $i$ -th line near the interference voltage terminal, and  $V_{i,FEXT}$  represents the disturbed voltage of the  $i$ -th line away from the interference voltage terminal.  $i = 2, 3, \dots, 9$ .

The crosstalk of the disturbed lines (#2, #3, #5, #6, #8, #9) in MTB-MTW is shown in Fig. 11 and Fig. 12, respectively. The solid line is the result obtained by the method proposed in this paper. The relevant parameters are shown in Table 1. The segmentation point of the FDTD algorithm is divided into 900 segments. The dashed line is the result of the CST simulation, and its arrangement is shown in Fig. 10.

It can be seen from Fig. 11 and 12 that the wires close to the interference wires (#2, #3) are more susceptible to interference than the wires far from the interference wires (#5, #6, #8, #9). Crosstalk between wires (#5, #6, #8, #9) far from the interference wires is very similar.

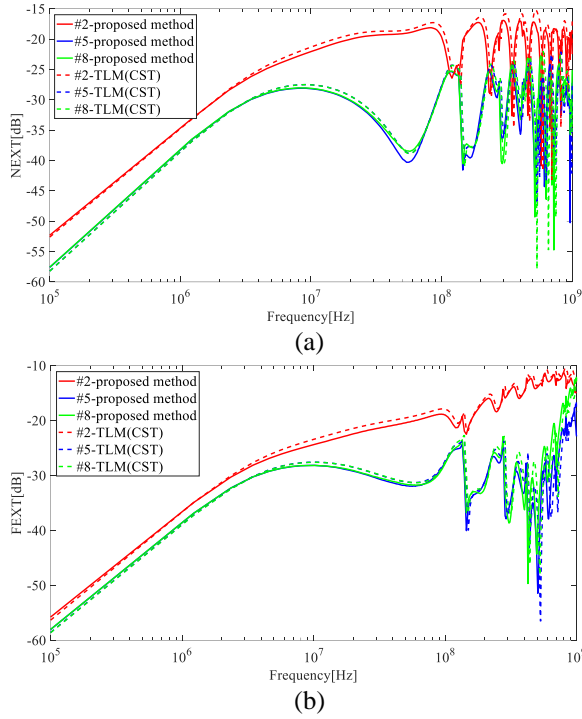


Fig. 11. Crosstalk prediction and simulation values of different bundle (#2, #5, and #8) in MTB-MTW. (a) NEXT and (b) FEXT.

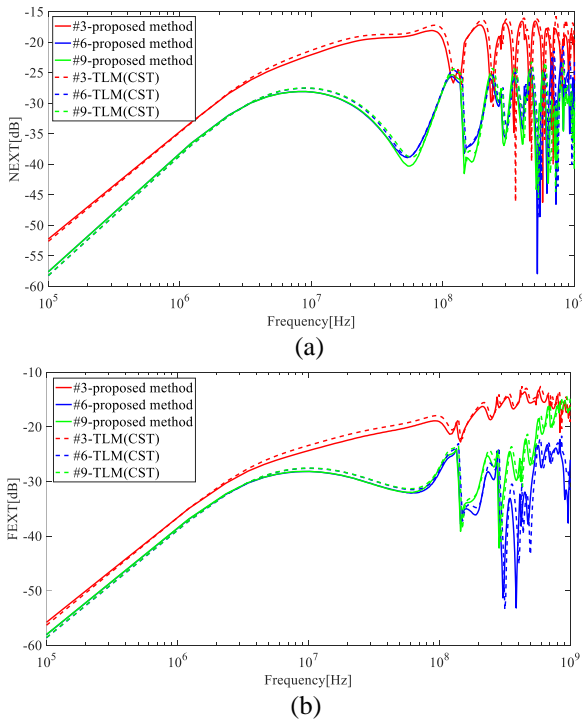


Fig. 12. Crosstalk prediction and simulation values of different bundle (#3, #6, and #9) in MTB-MTW. (a) NEXT and (b) FEXT.

In the frequency range below  $10^7$  MHz, the curve obtained by the proposed method and the TLM method agrees very well. In the frequency range higher than  $10^7$  MHz, the approximate contours of the images obtained by the new method and the TLM method are very similar, but the deviations at each frequency point are 0~3dB. This may not take into account that the parameter matrix will change with frequency.

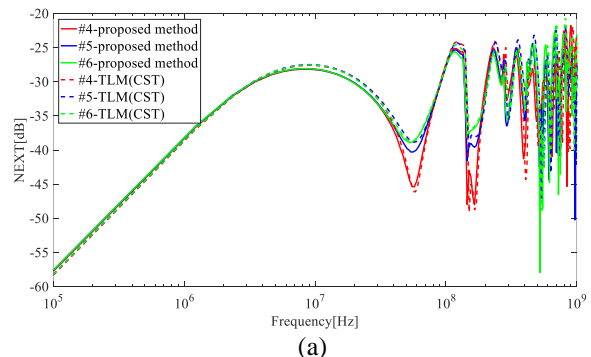
Tables 2 and 3 are the average error percentages between the results of the method proposed in this paper and those obtained by TLM. In the frequency ranges of 0.1~100 MHz, 100~500 MHz, and 500~1000 MHz, the maximum average errors are 4.508%, 13.800%, and 10.536%, respectively. From the perspective of average error, the results of the new method are more accurate in the low frequency and high frequency ranges.

Table 2: Average error (%) of different wires (NEXT)

Frequency (MHz)	0.1~100	100~500	500~1000
#2	3.730	12.436	10.010
#3	3.684	13.800	8.082
#4	1.584	7.960	3.703
#5	2.011	7.638	8.048
#6	1.107	5.944	8.642
#7	1.799	10.771	6.150
#8	1.017	7.727	10.536
#9	2.025	7.551	7.961

Table 3: Average error (%) of different wires (FEXT)

Frequency (MHz)	0.1~100	100~500	500~1000
#2	4.508	4.900	2.721
#3	4.446	4.727	2.912
#4	1.208	4.238	2.143
#5	1.787	7.879	6.988
#6	1.800	10.981	3.487
#7	1.318	4.627	2.764
#8	1.494	10.562	6.174
#9	1.849	7.303	2.831



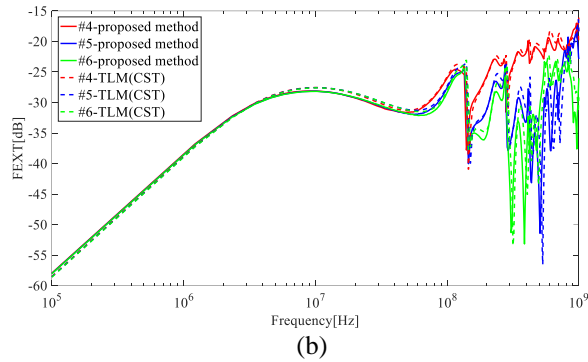


Fig. 13. Crosstalk prediction and simulation values of the bundle (#4, #5, and #6) in MTB-MTW. (a) NEXT and (b) FEXT.

In addition to the crosstalk curves of #5 and #8 (#6 and #9), it can be seen from Fig. 13 that the crosstalk curves of a bundle (#4, #5, #6) in the MTB-MTW are also very similar. The crosstalk curves of bundle (#7, #8, #9) in another MTB are also similar to Fig. 13. For the MTB-MTW model, the crosstalk between the wires is very close due to its double-layer twist. For the crosstalk suppression measures, only one wire condition needs to be considered, and the other wires are theoretically applicable.

## V. CONCLUSION

For the MTB-MTW model, this paper proposes a p.u.l parameter matrix prediction process based on the BSAS-BPNN algorithm and the Multilayer transposition method. And the FDTD method under Implicit-Wendroff difference format is combined to solve the crosstalk. In this paper, the twisted wires under the MTB-MTW model with  $n=N=3$  are studied and compared with the TLM method. The numerical experimental results first show that the iteration error of different p.u.l parameter matrices under the BSAS-BPNN algorithm can reach  $4 \times 10^{-6}$ ,  $5 \times 10^{-3}$ ,  $1 \times 10^{-3}$ , and  $2.5 \times 10^{-7}$ , respectively. Second, the proposed method is in good agreement with the NEXT and FEXT results of the TLM method at low and high frequencies. Finally, the results show that the crosstalk of the wires far away from the interference lines in MTB-MTW is very similar.

The method in this paper can be generalized to the MTB-MTW model of arbitrary conductors and twists, but the effect of frequency on the p.u.l parameter matrix and the non-uniform twisted wire model have not been considered. Therefore, there is still much research space after this paper.

## ACKNOWLEDGMENT

The paper is supported by National Natural Science Foundation of China (51475246), National Natural Science Foundation of Jiangsu Province (BK20161019),

and Aviation Science Foundation (20172552017).

## REFERENCES

- [1] C. R. Paul, "A brief history of work in transmission lines for EMC applications," *IEEE Trans. Electromagn. Compat.*, vol. 49, no. 2, pp. 237-252, May 2007.
- [2] S. Chabane, P. Besnier, and M. Klingler, "A modified enhanced transmission line theory applied to multiconductor transmission lines," *IEEE Trans. Electromagn. Compat.*, vol. 59, no. 2, pp. 518-528, Apr. 2017.
- [3] Y. Wang, Y. S. Cao, D. Liu, R. W. Kautz, N. Altunyurt, and J. Fan, "A generalized multiple-scattering method for modeling a cable harness with ground connections to a nearby metal surface," *IEEE Trans. Electromagn. Compat.*, vol. 61, no. 1, pp. 261-270, Feb. 2019.
- [4] C. P. Yang, W. Yan, Y. Zhao, Y. Chen, C. M. Zhu, and Z. B. Zhu, "Analysis on RLCG parameter matrix extraction for multi-core twisted cable based on back propagation neural network algorithm," *IEEE Access*, vol. 7, pp. 126315-126322, Aug. 2019.
- [5] O. Gassab and W. Y. Yin, "Characterization of electromagnetic wave coupling with a twisted bundle of twisted wire pairs (TBTWPs) above a ground plane," *IEEE Trans. Electromagn. Compat.*, vol. 61, no. 2, pp. 251-260, Feb. 2019.
- [6] C. D. Taylor and J. P. Castillo, "On the response of a terminated twisted-wire cable excited by a plane-wave electromagnetic field," *IEEE Trans. Electromagn. Compat.*, vol. EMC-22, no. 1, pp. 16-19, Feb. 1980.
- [7] Z. Fei, Y. Huang, J. Zhou, and C. Song, "Numerical analysis of a transmission line illuminated by a random plane-wave field using stochastic reduced order models," *IEEE Access*, vol. 5, pp. 8741-8751, May 2017.
- [8] Y. Yan, L. Meng, X. Liu, T. Jiang, J. Chen, and G. Zhang, "An FDTD method for the transient terminal response of twisted-wire pairs illuminated by an external electromagnetic field," *IEEE Trans. Electromagn. Compat.*, vol. 60, no. 2, pp. 435-443, Apr. 2018.
- [9] G. P. Veropoulos and P. J. Papakanellos, "A probabilistic approach for the susceptibility assessment of twisted-wire pairs excited by random plane-wave fields," *IEEE Trans. Electromagn. Compat.*, vol. 59, no. 3, pp. 926-969, June 2017.
- [10] G. Spadacini, F. Grassi, and S. A. Pignari, "Field-to-wire coupling model for the common mode in random bundles of twisted-wire pairs," *IEEE Trans. Electromagn. Compat.*, vol. 57, no. 5, pp. 1246-1254, Oct. 2015.
- [11] O. Gassab, L. Zhou, W. Y. Yin, and H. Xie,

- “Modelling electromagnetic wave coupling and mode conversion effects in multitwisted bundle of twisted-wire pairs (MTB-TWP) above ground plane,” *Int. J. Numer. Model. Electron. Netw. Devices Fields*, 2018, doi: 10.1002/jnm.2539.
- [12] C. R. Paul, *Analysis of Multiconductor Transmission Lines*. Hoboken, NJ, USA: Wiley, 1994.
- [13] P. Manfredi, D. De Zutter, and D. V. Ginste, “Analysis of nonuniform transmission lines with an iterative and adaptive perturbation technique,” *IEEE Trans. Electromagn. Compat.*, vol. 58, no. 3, pp. 859-867, June 2016.
- [14] G. Spadacini, “Numerical assessment of radiated susceptibility of twisted-wire pairs with random nonuniform twisting,” *IEEE Trans. Electromagn. Compat.*, vol. 55, no. 5, pp. 956-964, Oct. 2013.
- [15] C. Jullien, P. Besnier, M. Dunand, and I. Junqua, “Advanced modeling of crosstalk between an unshielded twisted pair cable and an unshielded wire above a ground plane,” *IEEE Trans. Electromagn. Compat.*, vol. 55, no. 1, pp. 183-194, Feb. 2013.
- [16] A. Shoory, M. Rubinstein, A. Rubinstein, and F. Rachidi, “Simulated NEXT and FEXT in twisted wire pair bundles,” *In Proc. EMC Eur. Symp.*, York, U.K., pp. 266-271, Sep. 2011.
- [17] M. Tang and J. Mao, “A precise time-step integration method for transient analysis of lossy nonuniform transmission lines,” *IEEE Trans. Electromagn. Compat.*, vol. 50, no. 1, pp. 166-174, Feb. 2018.
- [18] A. Tatematsu, F. Rachidi, and M. Rubinstein, “A technique for calculating voltages induced on twisted-wire Pairs Using the FDTD method,” *IEEE Trans. Electromagn. Compat.*, vol. 59, no. 1, pp. 301-304, Feb. 2017.
- [19] V. R. Kumar, B. K. Kaushik, and A. Patnaik, “An accurate FDTD model for crosstalk analysis of CMOS-Gate-Driven coupled RLC interconnects,” *IEEE Trans. Electromagn. Compat.*, vol. 56, no. 5, pp. 1185-1193, Oct. 2014.
- [20] B. Cannas, A. Fanni, and F. Maradei, “A neural network approach to predict the crosstalk in non-uniform multi-conductor transmission lines,” *IEEE In. Symp. on Circuits. and Systems*, Phoenix-Scottsdale, AZ, USA, pp. 573-576, May 2002.
- [21] F. Dai, G. H. Bao, and D. L. Su, “Crosstalk prediction in non-uniform cable bundles based on neural network,” *Proceedings of the 9th In Symp. on Antennas, Propagation and EM Theory*, Guangzhou, China, pp. 1043-1046, 2010.
- [22] J. Wang and H. Chen, “BSAS: Beetle swarm antennae search algorithm for optimization problems,” *arXiv preprint. arXiv:1807.10470*, 2018.018, 51(11):60-66.
- [23] Q. Wu, Z. Ma, G. Xu, S. Li, and D. Chen, “A novel neural network classifier using beetle antennae search algorithm for pattern classification,” *IEEE Access*, vol. 7, pp. 64686-64696, May 2019.
- [24] L. Dou and J. Dou, “Time-domain analysis of lossy multiconductor transmission lines based on the Lax-Wendroff technique,” *Analog Integrated Circuits and Signal Processing*, vol. 68, no. 1, pp. 85-92, 2011.
- [25] C. Che, H. P. Zhao, Y. D. Guo, J. Hu, and H. Kim, “Investigation of segmentation method for enhancing high frequency simulation of Q3D extractor,” *IEEE In Conference on Computational Electromagn (ICCEM)*, Shanghai, China, Mar. 2019.
- [26] CST Microwave Studio, ver. 2008, Computer Simulation Technology, Framingham, MA, 2008.



**Chao Huang** was born in Anhui Province, China. He received the B.S degree in School of electrical Engineering and Automation from Anhui University of Technology, Maanshan, China, in 2018. He is currently working toward the Master's degree in Electrical Engineering at Nanjing Normal University, Nanjing, China. His main research interests include multi-conductor transmission lines and EMC.



**Yang Zhao** received his B.E., M.E., and Ph.D. degree all in Power Electronic Technology from Nanjing University of Aeronautics and Astronautics, Nanjing, China, in 1989 and 1992, and 1995, respectively. He is currently the Professor with Nanjing Normal University. His research interests are in the areas of Electromagnetic Compatibility, Power Electronics and Automotive Electronics.



**Wei Yan** Doctor & Assoc. Professor from Nanjing Normal University. He obtained the Physics and Electronics Ph.D. and Electrical Engineering M.S. from Nanjing Normal University in 2014 and 2011. He is the Senior Member of China Electrical Technology Association and the evaluation expert of the Electromagnetic Compatibility Calibration Specification of China.



**Qiangqiang Liu** was born in Anhui Province, China. He received the B.S. degree in School of Electrical Engineering and Automation from Anhui University of Science and Technology, Huainan, China, in 2018. He is currently working toward the Master's degree in Electrical Engineering at Nanjing Normal University, Nanjing, China. His major research interests include new technology of electrical engineering.